International Symposium
On Turbulence and Shear Flow
Phenomena (TSFP-9)
June 30 - July 3, 2015 *Melbourne, Australia*

EFFECTS OF TAYLOR-GÖRTLER VORTICES ON NEAR-WALL COHERENT STRUCTURES

Zixuan Yang
Dept. of Mechanical Engineering
Univ. of Manitoba
Winnipeg, MB, R3T 3M2, Canada
yangz348@ad.umanitoba.ca

Bing-Chen Wang
Dept. of Mechanical Engineering
Univ. of Manitoba
Winnipeg, MB, R3T 3M2, Canada
BingChen.Wang@ad.umanitoba.ca

ABSTRACT

In this paper, direct numerical simulations (DNS) have been performed to investigate the superimposition and modulation effects of Taylor-Görtler (TG) vortices on near-wall coherent structures in the context of streamwise-rotating turbulent channel flow. The evolution and dynamic interaction of the TG vortices with near-wall streaks have been studied in both spectral and physical spaces. An interesting bimodal pattern is observed in the pre-multiplied energy spectra which effectively differentiates the characteristic length scales of near-wall streaks from those of TG vortices. In the physical space, it is discovered that the near-wall streaks are influenced by the superimposition effect of TG vortices, and vary quasi-periodically in the spanwise direction. It is also interesting to observe that with positive and negative superimposition effects of TG vortices, the intensity of streaks is enhanced and reduced, respectively, clearly revealing that TG vortices has an amplitude-modulation effect on the near-wall structures.

INTRODUCTION

Turbulent flows subjected to system rotations are of considerable interests in a variety of engineering and geophysical applications, such as design of turbo jets and rotary machines, and prediction of cyclones and ocean currents. In response to the system rotation, Coriolis forces appear as non-conservative forces, acting on the fluid and inducing large longitudinal secondary flows, so-called TG vortices. The appearance of TG vortices significantly alters the turbulent flow structures, and as a consequence, the transport processes of momentum and energy in rotating flows are subject to further flow-structure related dynamical complexities. The TG vortices in the spanwise-rotating turbulent channel flow were first observed in the experiment conducted by Johnston *et al.* (1972). Since then, extensive numerical simulations have been conducted in order to understand the physics of both spanwise- and streamwise-rotating turbulent channel flows, which include the DNS studies of Kristoffersen & Andersson (1993) and Weller & Oberlack (2006), and large-eddy simulation (LES) studies of Pallares & Davidson (2002) and Wang & Zhang (2013).

Based on their experiment conducted in a high-Reynolds-number boundary-layer wind-tunnel at the University of Melbourne, Mathis *et al.* (2009) concluded that in turbulent boundary layers, the large energetic vortices in the outer-layer interacts with near-wall flow structures through the so-called "superimposition" and "modulation" effects. The concept of superimposition effect was first proposed by Townsend (1976), who predicted that large-scale outer-layer motions could leave a footprint on near-wall structures due to the attached eddies centered in the outer layer, such that the scale of structures far above the wall were superimposed onto the near-wall small-scale structures. The prediction of Townsend (1976) was later confirmed by Metzger & Klewicki (2001) based on analyzing the experimental data measured in a wind tunnel and in the atmospheric boundary layer. Later, Hutchins & Marusic (2007) observed that in addition to the superimposition effect, the large scales can further modulate the magnitude of small-scale fluctuations. They indicated that in the near-wall region directly influenced by high-speed outer-layer large-scale structures, small-scale fluctuations are typically enhanced. Yang *et al.* (2012) conducted a LES study of spanwise-rotating turbulent channel flows and concluded that the occurrence of the TG vortices alters the pattern of near-wall streaks significantly. In their most recent LES study of a streamwise-rotating flow, Wang & Zhang (2013) observed that although the TG vortices are predominant in the central core of the channel, they have a significant influence on the wall-frictional velocity. The mechanism underlying this observation lies in the superimposition effect of the TG vortices on near-wall coherent structures.

Notwithstanding the relevant contributions reviewed above, the dynamic interactions of TG vortices with near-wall coherent structures have not been thoroughly studied in literature, and thus far, it has not been clear whether TG vortices may impose modulation effects on the streaks. In

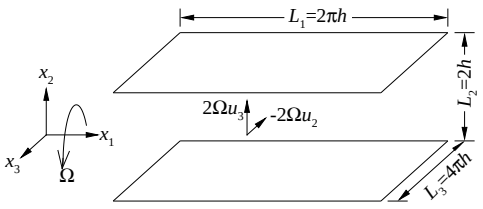

Figure 1. Computational domain for a streamwise-rotating channel flow.

view of this, we perform DNS of streamwise-rotating turbulent channel flows at very high rotation numbers, for which TG vortices can be observed clearly. We report solid evidence on the superimposition and modulation effects of TG vortices on near-wall streaks. The effect of TG vortices are thoroughly discussed in both spectral and physical spaces.

TEST CASES AND NUMERICAL ALGORITHM

Figure 1 shows the computational domain and coordinate system of the streamwise-rotating turbulent channel flow. The streamwise, wall-normal and spanwise coordinates are denoted using x_1, x_2 and x_3, respectively, and u_1, u_2 and u_3 represent velocity components in corresponding directions. As shown in Fig. 1, due to the imposed system rotation, the Coriolis force appears, which includes two non-trivial components $f_2 = 2\Omega u_3$ and $f_3 = -2\Omega u_2$. Here Ω represents the angular velocity of the system rotation. Under the influence of the Coriolis force, TG vorticies are induced, which appear as large secondary flows and drastically alter the flow dynamics of the channel flow. The effects of TG vortices are analyzed based on two rotation numbers for $Ro = 2\Omega h/u_m = 7.5$ and 15.0, where h represents the half channel width, and u_m represents the bulk mean velocity. These two rotation numbers are significantly higher than those considered in previous literature on streamwise-rotating turbulent channel flows. For instance, in Weller & Oberlack (2006), the rotation number tested was about $Ro = 1$. Owing to the high rotation number tested in current simulations, the influences of TG vortices can be observed clearly. The Reynolds number for these two cases is fixed to $Re = u_m h/\nu = 7000$, where ν represents the kinematic viscosity of the fluid.

The dimensions of the computational domain are $L_1 \times L_2 \times L_3 = 2\pi h \times 2h \times 4\pi h$ and the numbers of resolved wavenumbers in spectral space are set to $N_1 \times N_2 \times N_3 = 384 \times 256 \times 1536$ for both test cases. The spanwise domain size of the present channel is 4 times that used by Moser *et al.* (1999) in their DNS study of a non-rotating turbulent channel flow of the same Reynolds number. This is because in the context of a streamwise-rotating channel flow, TG vortices are induced by the Coriolis force, which appear in pairs and dominate the flow structures in the cross-stream directions. In order to study the statistics of TG vortex motions and to capture their dynamics at the lowest spatial and temporal frequencies, there is a need to extend the spanwise domain size to include more TG vortex pairs. Furthermore, in comparison with the non-rotating channel case of Moser *et al.* (1999), the grid resolution in the current simulations is significantly refined. This is because the turbulence level is enhanced by the imposed streamwise rotation, especially in the near-wall region.

The continuity and momentum equations that govern the motion of incompressible fluid subjected to a system rotation are solved using an in-house pseudo-spectral method code. All quantities are expanded into Fourier series in streamwise-spanwise (x_1-x_3) planes, and into Chebyshev polynomial series in the wall-normal (x_2) direction. The convection terms in momentum equations are calculated in physical space, and the aliasing errors are eliminated by applying the 3/2 rule. The time advancement is achieved using a standard 3rd-order time-splitting method of Karniadakis *et al.* (1991). Details of the numerical algorithm can be found in Yang *et al.* (2012).

RESULTS ANALYSIS

Statistical properties of TG vortices

Before we start analyzing the effect of TG vortices on near-wall structures, fundamental properties of the TG vortices need to be addressed. Because TG vortices are persistent and streamwise-elongated, it is proper to visualize them based on time- and streamwise-averaging (SA). Figure 2 shows the vector map of velocity fluctuations $[\tilde{u}_2']$-$[\tilde{u}_3']$ in a x_2-x_3 plane. Here, the square brackets and tilde represent time and streamwise averaging, respectively. From Fig. 2, 5 and 4 pairs of large-scale roll cells can be observed in the cross-stream plane at $Ro = 7.5$ and $Ro = 15.0$, respectively.

Kristoffersen & Andersson (1993) indicated that because SA fluctuations ($\tilde{u}_i'$) do not converge to zero even under a very long time averaging, it is not reasonable to treat them as real fluctuations. They suggested that the total fluctuations be decomposed into the SA fluctuations and real fluctuations $\tilde{u}_i''$, i.e.

$$u_i' = u_i'' + \tilde{u}_i' \quad . \tag{1}$$

Based on this decomposition, the turbulence kinetic energy (TKE) can be also decomposed into two parts as

$$k = k_{\mathrm{TG}} + k_{\mathrm{real}} \quad , \tag{2}$$

where $k = \frac{1}{2}\langle u_i' u_i' \rangle$, $k_{\mathrm{TG}} = \frac{1}{2}\langle \tilde{u}_i' \tilde{u}_i' \rangle$ and $k_{\mathrm{real}} = \frac{1}{2}\langle u_i'' u_i'' \rangle$ represent TKE of the total, SA and real fluctuations, respectively.

Figure 3 compares the profiles of k, k_{TG} and k_{real} at $Ro = 15.0$. From the figure, it is clear that k_{real} dominates in the near-wall region. As the distance from the wall increases, k_{TG} becomes more prominent. This can be attributed to fact that TG vortices occur in the center core of the channel. In addition to the two near-wall peaks, another peak occurs in the profile of TKE in the central vertical plane (located at $x_2/h = 0$). By comparing the profiles of k_{TG} and k_{real}, it is evident that this central peak is caused by the occurrence of the TG vortices.

Superimposition effect of TG vortices

In order to demonstrate the effects of TG vortices on near-wall structures, we study the streaks in plane $x_2^+ = 10$. Figure 4(a) displays the streaks at $Ro = 7.5$ using the contours of instantaneous total streamwise fluctuations $u_1'^+$. As marked in the figure using letters "L" and "H", 5 low-speed and 5 high-speed regions alternate quasi-periodically along the x_3 direction. As shown in Fig. 4(b), when the rotation

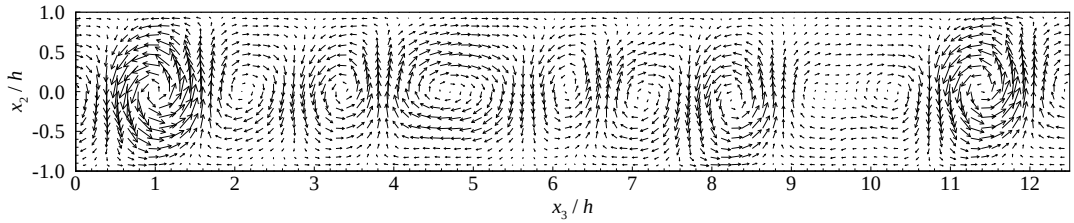

(a) $Ro = 7.5$

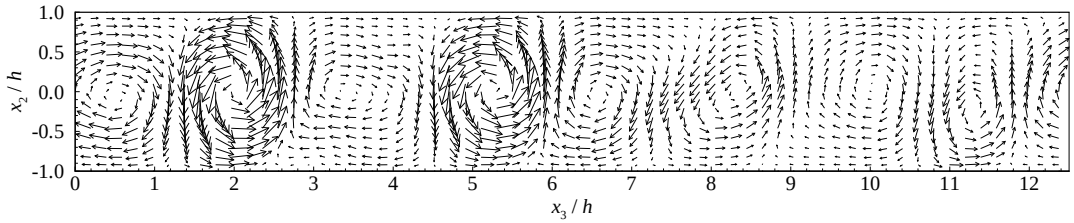

(b) $Ro = 15.0$

Figure 2. TG vortices demonstrated using vectors of time and streamwise-averaged total velocity fluctuations $[\tilde{u}_2']$-$[\tilde{u}_3']$ in a x_2-x_3 plane.

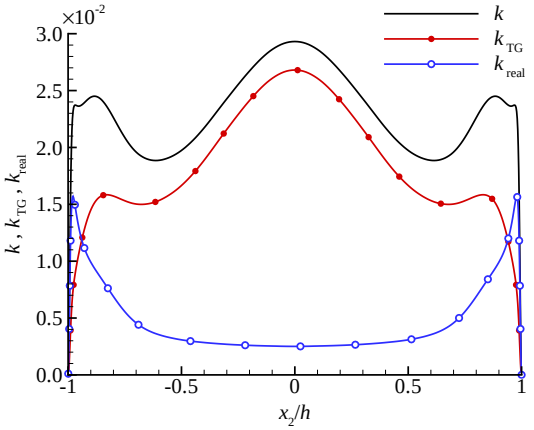

Figure 3. Profiles of TKE of the total, SA and real fluctuations at $Ro = 15.0$.

number increases from 7.5 to 15.0, a similar alternating pattern of low- and high-speed streaks can be observed, but the number of the quasi-periods is reduced from 5 to 4. These numbers of the quasi-periods of near-wall streaks at two rotation numbers are identical to those of TG vortices pairs shown previously in Fig. 2, which indicates that the quasi-periodical distribution of low- and high-speed streaks is directly correlated to the occurrence of the TG vortices.

Figure 5 displays the contours of the streamwise real fluctuation u_1'' in plane $x_2^+ = 10$ at $Ro = 15.0$. It is clear that the spanwise scale of the streaks exhibited in Fig. 5 for the real fluctuations is significantly smaller than that exhibited in Fig. 4(b) for the total fluctuations. This confirms that the large-scale near-wall streaks observed in Fig. 4(b) indeed directly correlate to the TG vortices, indicating the superimposition effect of the TG vortices on the near-wall flow structures. Figure 5 also indicates that the decomposition given by Eq. (1) is effective for demonstrating the superimposition effect of the TG vortices.

The superimposition effect demonstrated above indi-

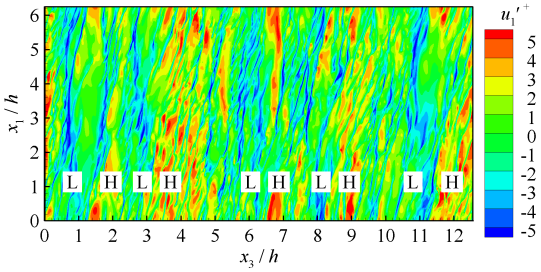

(a) $Ro = 7.5$

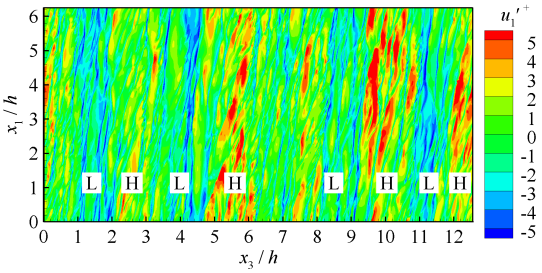

(b) $Ro = 15.0$

Figure 4. Contours of instantaneous streamwise fluctuation $u_1'^+$ in plane $x_2^+ = 10$ for streamwise-rotating cases. Low- and high-speed streaks are marked by "L" and "H", respectively.

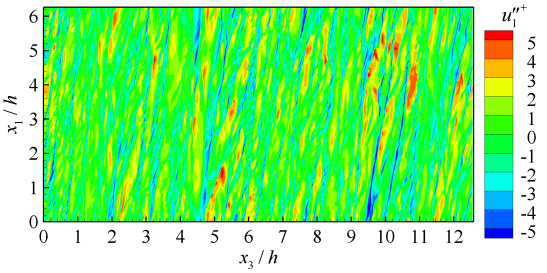

Figure 5. Contours of instantaneous streamwise real fluctuation $u_1''^+$ in plane $x_2^+ = 10$ at $Ro = 15.0$.

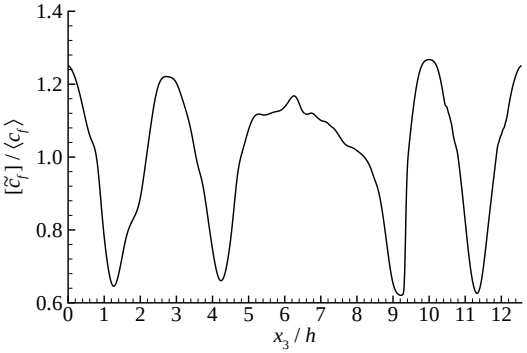

Figure 6. Spanwise profile of the time and streamwise-averaged wall-frictional coefficient at $Ro = 15.0$.

cates that although the TG vortices appear in the central core of the channel, they are 'seen' in the near-wall region. As a result, the scale of TG vortices is superimposed on not only near-wall streaks, but also the wall shear stress. To demonstrate, we consider the wall-frictional coefficient, defined as

$$c_f = \frac{\mu \left.\dfrac{\partial u_1}{\partial x_2}\right|_{x_2=-h}}{\dfrac{1}{2}\rho u_m^2} \quad . \tag{3}$$

Figure 6 displays the spanwise profile of the time- and streamwise-averaged wall-frictional coefficient $[\tilde{c}_f]$ at $Ro = 15.0$. The value of $[\tilde{c}_f]$ shown in the figure is normalized using the mean wall-frictional coefficient $\langle c_f\rangle$. As shown in the figure, due to the superimposition effect of the TG vortices, altogether 4 periods can be observed in the profile of $[\tilde{c}_f]$ across the entire spanwise domain. By comparing Fig. 6 with Fig. 4(b), it is clear that in the region that dominated by high-speed streaks (for example, around $x_3/h = 10.0$), the value of $[\tilde{c}_f]/\langle c_f\rangle$ is greater than 1, indicating that the wall shear stress is enhanced. In contrast, in the region with low-speed streaks (for example, around $x_3/h = 11.3$), the wall shear stress is suppressed, characterized by $[\tilde{c}_f]/\langle c_f\rangle < 1$. The ratio of $[\tilde{c}_f]$ to $\langle c_f\rangle$ varies between 0.6 to 1.3, indicating that the TG vortices influences the magnitude of the wall shear stress by approximately 35%.

According to the decomposition of TKE given by Eq. (2), the 1-dimensional (1D) spanwise energy spectrum $E(k_3)$ can be also decomposed into the energy spectrum of the SA fluctuations $E_{\mathrm{SA}}(k_3)$ and that of the real fluctuations $E_{\mathrm{real}}(k_3)$, where k_3 represents the spanwise wavenumber. Figure 7 compares the spanwise pre-multiplied energy spectra of total fluctuations $k_3E(k_3)$, SA fluctuations $k_3E_{\mathrm{SA}}(k_3)$ and real fluctuations $k_3E_{\mathrm{real}}(k_3)$ at $Ro = 15.0$. Figure 7(a) displays the energy spectra in the central x_1-x_3 plane ($x_2/h = 0$). As shown in the figure, a single peak appears at $k_3 = 2$ in the profile of $k_3E(k_3)$, which is primarily contributed by the SA fluctuations associated with TG vortices in the channel center. Wavenumber $k_3 = 2$ corresponds to a spanwise scale of $2\pi/2 = \pi$. As such within the 4π spanwise domain, 4 pairs of TG vortices are expected, which is in excellent conformance with the observation from Fig. 2(b).

In the near-wall region (for $x_2^+ = 10$), as shown in Fig. 7(b), the pre-multiplied energy spectra of total fluctuations exhibits a bimodal shape. One peak occurs at $k_3 \approx 15$, which corresponds to the spanwise characteristic scale of streaks contributed mainly by the real fluctuations. The other peak appears at wavenumber $k_3 = 2$. By comparing Fig. 7(a) with 7(b), it is evident that the scale of TG vortices (characterized by wavenumber $k_3 = 2$) has been superimposed onto the near-wall streaks.

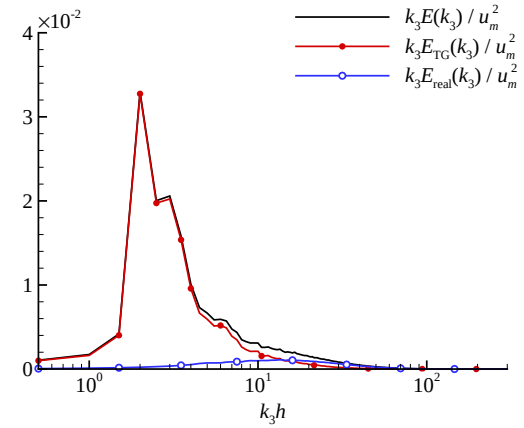

(a) central plane at $x_2/h = 0$

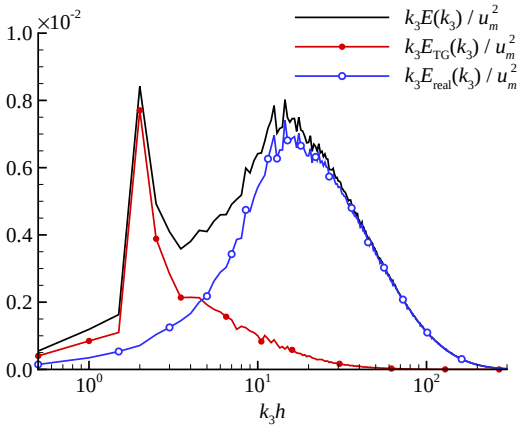

(b) near-wall plane at $x_2^+ = 10$

Figure 7. Premultiplied 1D energy spectra of total, SA and real streamwise fluctuations against spanwise wavenumber k_3 in central and near-wall x_1-x_3 planes for $Ro = 15.0$.

Modulation effect of TG vortices

In order to demonstrate the modulation effect of TG vortices, isopleths of the streamwise real fluctuation with very large magnitude (for $|u_1''^+| = 4$) are plotted in Fig. 8. Letters "L" and "H" represent the low and high speed streak regions with negatively and positively valued SA fluctuation $\tilde{u}_1'$, respectively (see also Fig. 4(b)). As shown in Fig. 8, in the regions with positively valued $\tilde{u}_1'$, isopleths of $|u_1''^+| = 4$ are concentrated, whereas in the regions with negatively valued $\tilde{u}_1'$, significantly fewer such isopleths can be observed. This indicates that the positively and negatively valued $\tilde{u}_1'$ enhances and suppresses real fluctuations, respectively. In other words, the amplitude of $u_1''^+$ is modulated by $\tilde{u}_1'$.

The modulation effect can be further quantitatively analyzed based on conditional statistics. To this purpose, we define operators $\langle\cdot\rangle_-$ and $\langle\cdot\rangle_+$ as averaging under conditions $\tilde{u}_1' < 0$ and $\tilde{u}_1' > 0$, respectively.

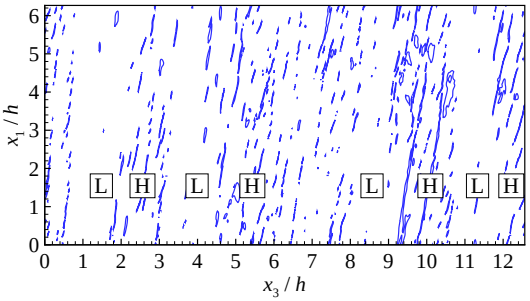

Figure 8. Isopleths of instantaneous streamwise real fluctuation with very large magnitude ($|u_1''^+| = 4$) in plane $x_2^+ = 10$ at $Ro = 15.0$. Letters "L" and "H" indicate spanwise regions with negative and positive $\tilde{u}_1'$.

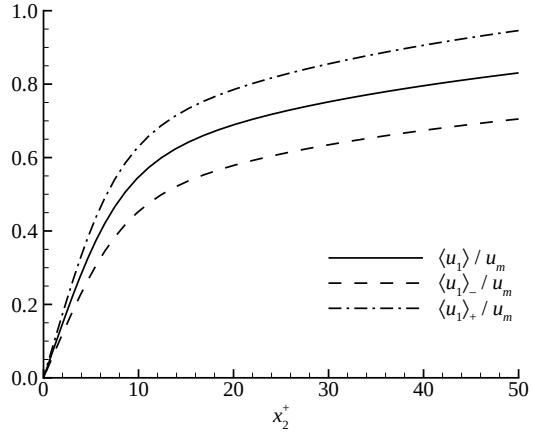

Figure 9. Profiles of $\langle u_1\rangle$, $\langle u_1\rangle_-$ and $\langle u_1\rangle_+$ in the near-wall region (for $x_2^+ \leq 50$) at $Ro = 15.0$.

Figure 9 compares the profiles of $\langle u_1\rangle$, $\langle u_1\rangle_-$ and $\langle u_1\rangle_+$ in the near-wall region (for $x_2^+ \leq 50$) at $Ro = 15.0$. From the figure, it is clear that $\langle u_1\rangle_+ > \langle u_1\rangle > \langle u_1\rangle_-$, which indicates that the mean shear under condition $\tilde{u}_1' > 0$ is larger than that under condition $\tilde{u}_1' < 0$. It is known that the mean shear $d\langle u\rangle/dy$ is important for the production of TKE in the wall-bounded turbulence. Therefore, the turbulence level is higher under condition $\tilde{u}_1' > 0$ than that under condition $\tilde{u}_1' < 0$ (see also, Fig. 8).

Figure 10 compares the profiles of k_{real} , $k_{\text{real}-}$ and $k_{\text{real}+}$. Here $k_{\text{real}-} = \frac{1}{2}\langle u_i'' u_i''\rangle_-$ and $k_{\text{real}+} = \frac{1}{2}\langle u_i'' u_i''\rangle_+$ represent TKE of real fluctuations under condition $\tilde{u}_1' < 0$ and $\tilde{u}_1' > 0$, respectively. As expected, the value of TKE under conditions $\tilde{u}_1' > 0$ and $\tilde{u}_1' < 0$ is higher and lower than the averaging value of TKE, respectively, i.e. $k_{\text{real}+} > k_{\text{real}} > k_{\text{real}-}$. In plane $x_2^+ = 10$, the magnitude of k_{real}/u_m^2 is about 2.52×10^{-2}, whereas those of $k_{\text{real}-}/u_m^2$ and $k_{\text{real}+}/u_m^2$ are about 2.18×10^{-2} and 2.82×10^{-2}, respectively, and as such, the TG vortices modulate the amplitude of TKE by approximately 12.6%. The results of TKE of real fluctuations displayed in Fig. 10 confirms that the TG vortices modulate the amplitude of the real fluctuations, and therefore, real fluctuations with very large magnitudes are concentrated in regions where $\tilde{u}_1'$ is positively valued (see, Figs. 4(b) and 8).

The mechanism underlying the modulation effect lies in the variation of the production of TKE in different region in response to the TG vortical motions. Figure 11 compares the profiles of P_k, P_{k-} and P_{k+}, where $P_k = -d\langle u_1\rangle/dx_2 \cdot \langle u_1' u_2'\rangle$, $P_{k-} = -d\langle u_1\rangle/dx_2 \cdot \langle u_1' u_2'\rangle_-$ and $P_{k+} = -d\langle u_1\rangle/dx_2 \cdot \langle u_1' u_2'\rangle_+$ represent the mean production of TKE, production of TKE under condition $\tilde{u}_1' < 0$ and that under condition $\tilde{u}_1' > 0$, respectively. As shown in the figure, the production term exhibits a similar behavior of TKE discussed previously in Fig. 10, such that $P_{k+} > P_k > P_{k-}$. This indicates that the modulation effect of the TG vortices is also imposed onto the production of TKE. Furthermore, the modulation effect on P_k is even stronger than that on the TKE exhibited in Fig. 10. In plane $x_2^+ = 10$, The values of $P_k/(u_m^3/h)$, $P_{k-}/(u_m^3/h)$ and $P_{k+}/(u_m^3/h)$ are 3.1×10^{-2}, 4.5×10^{-2} and 5.9×10^{-2}, respectively. The magnitude of $P_{k+}/(u_m^3/h)$ is almost twice that of $P_{k-}/(u_m^3/h)$, indicating that the TG vortices modulate P_k by approximately 30%.

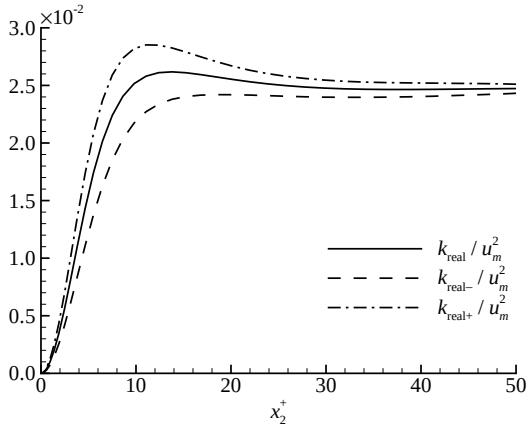

Figure 10. Profiles of k_{real} , $k_{\text{real}-}$ and $k_{\text{real}+}$ in the near-wall region (for $x_2^+ \leq 50$) at $Ro = 15.0$.

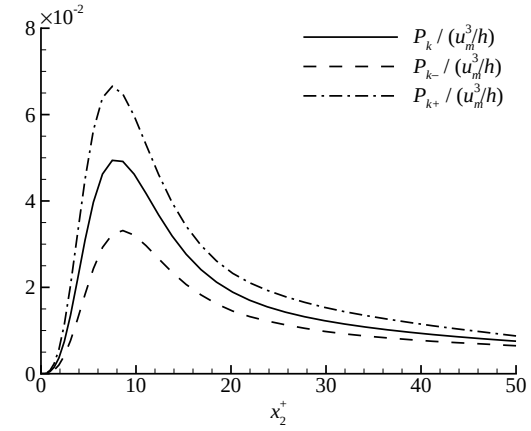

Figure 11. Profiles of k_{real} , $k_{\text{real}-}$ and $k_{\text{real}+}$in the near-wall region ($x_2^+ \leq 50$) at $Ro = 15.0$.

Conclusions

DNS has been performed to investigate the superimposition and modulation effects of the TG vortices on the near-wall streaks in the context of streamwise-rotating turbulent channel flows in both physical and spectral spaces. Although the TG vortices are located in the central region of the channel, their scales are superimposed onto the near-wall streaks, such that the high-speed and low-speed streaks appear

quasi-periodically in the spanwise direction, and the mean spanwise size of such periods is consistent with that of TG vortex pairs. A bimodal shape in the pre-multiplied spanwise energy spectrum is observed in the near-wall region, with one peak corresponding to the spanwise scale of TG vortices and the other corresponding to that of real fluctuations.

In addition to the superimposition effect, the TG vortices also modulate the amplitude of the real fluctuations. Based on the conditional averaging method, it is observed that in regions with positive and negative SA fluctuations of $\tilde{u}_1'$, the real fluctuation level is enhanced and suppressed, respectively. The modulation effect can be attributed to fact that in the region for $\tilde{u}_1' > 0$, the shear stress is stronger and the production term of TKE is of larger magnitudes.

Through this research, solid evidences on the superimposition and modulation effects of the TG vortices on near-wall flow structures are obtained. However, a concrete functional relationship between the TG vortices and real fluctuations still remains unknown. To solve this problem, the Hilbert transform needs to be utilized for decomposing large and small scale structures, and we plan to continue on this research direction in the near future.

REFERENCES

Hutchins, N. & Marusic, I. 2007 Large-scale influences in near-wall turbulence. *Phil. Trans. R. Soc. Lond. A* **365**, 647–664.

Johnston, J. P., Halleen, R. M. & Lezius, D. K. 1972 Effects of spanwise rotation on the structure of two-dimensional fully developed turbulent channel flow. *J. Fluid Mech.* **56**, 533–559.

Karniadakis, G. E., Israeli, M. & Orszag, S. A. 1991 High-order splitting methods for the incompressible Navier-Stokes equations. *J. Comput. Phys.* **97(2)**, 414–443.

Kristoffersen, R. & Andersson, H. I. 1993 Direct simulations of low-Reynolds-number turbulent flow in a rotating channel. *J. Fluid Mech.* **256**, 163–197.

Mathis, R., Hutchins, N. & Marusic, I. 2009 Large-scale amplitude modulation of the small-scale structures in turbulent boundary layers. *J. Fluid Mech.* **628**, 311–337.

Metzger, M. M. & Klewicki, J. C. 2001 A comparative study of near-wall turbulence in high and low Reynolds number boundary layers. *Phys. Fluids* **13**, 692–701.

Moser, R. D., Kim, J. & Mansour, N. N. 1999 Direct numerical simulation of turbulent channel flow up to $Re_\tau = 590$. *Phy. Fluids* **11**, 943–945.

Pallares, J. & Davidson, L. 2002 Large-eddy simulations of turbulent heat transfer in stationary and rotating square ducts. *Phys. Fluids* **14**, 2804–2816.

Townsend, A. A. 1976 *The Structure of Turbulent Shear Flow*, 2nd edn. Cambridge University Press.

Wang, B.-C. & Zhang, Y. 2013 Large-eddy simulation of turbulent flows in a heated streamwise rotating channel. *Int. J. Heat Fluid Flow.* **44**, 71–86.

Weller, T. & Oberlack, M. 2006 DNS of a turbulent channel flow with streamwise rotation - study of the reverse effect of the cross flow. *Proc. Appl. Math. Mech.* **6**, 553–554.

Yang, Z., Cui, G., Xu, C.-X. & Zhang, Z.-S. 2012 Large eddy simulation of rotating turbulent channel flow with a new dynamic global-coefficient nonlinear subgrid stress model. *J. Turbulence* **13**, No. 48.